Journal Name

Synthesis, Structure and Photocatalytic Activity of Layered $LaOInS_2$

,Received 00th January 20xx,
Accepted 00th January 20xx

DOI: 10.1039/x0xx00000x

www.rsc.org/

Akira Miura[a*], Takayoshi Oshima [b,c], Kazuhiko Maeda[b*], Yoshikazu Mizuguchi[d], Chikako Moriyoshi[e], Yoshihiro Kuroiwa[e], Yu Meng[f,g], Xiao-Dong Wen[f,g], Masanori Nagao[h], Mikio Higuchi[a], Kiyoharu Tadanaga[a]

Indium oxychalcogenides would be attractive semiconductors considering the practical use of indium oxides and sulfides such as indium-tin oxides (ITO) and copper-indium-gallium diselenides (CIGS). In this work, a novel layered indium oxysulfide, $LaOInS_2$, was synthesized by a metathesis reaction between LaOCl and $NaInS_2$. Synchrotron X-ray diffraction showed that $LaOInS_2$ consisted of alternately stacked rocksalt-type In–S and PbO-type La–O layers. InS_6 octahedron had splitting In sites with abnormally large anisotropic atomic displacement factors. $LaOInS_2$ was found to be a direct semiconductor. Density functional theory calculations exhibited well-dispersed bands composed of In 5s/5p and S 3p/O 2p orbitals with a band gap of ~2.4 eV, which was close to the experimental value estimated by optical absorption (2.64 eV). By responding this visible-light absorption, $LaOInS_2$ exhibited photocatalytic activity for H_2 and O_2 evolution from water with the aid of Pt and IrO_2 cocatalysts, respectively

Introduction

Oxychalcogenides have been studied extensively because coexistence of ionic oxide anions and chalcogenide anions often adopt both low-dimensional structure and anisotropic electronic structure together with various applications.[1-5] For instance, $Sm_2Ti_2S_2O_5$ adopts the layered structure similar to a Ruddlesden–Popper-type layered perovskite oxide, and it acts as a water splitting photocatalyst under visible light.[6] LaOAgS consists of alternate stacking of La-O and Ag-S layers, and is an excellent ion conductor.[7] Isostructural LaOCuS has been found to be a p-type semiconductor with a band gap of 3.2 eV.[8] Some researchers have studied bismuth oxychalcogenides containing Bi-S/Se layer, such as $LaOBiS_2$ and $LaOBi(S,Se)_2$, and their superconductive and thermoelectric properties have been examined.[9-14] The crystallographic structure of $LaOBiS_2$ can be characterized as a distorted rocksalt-based Bi-S layer sandwiched by La-O blocks. Low-dimensional and covalent Bi-S layers form highly dispersed bands, which acts a superconductive layer by inducing electronic carrier properties.[10-12] Abnormally high thermal vibration of Bi-Se layers has been detected in $LaOBi(S,Se)_2$, which is advantageous for thermoelectric materials.[13]

Indium oxides and chalcogenides, including indium tin oxides (ITO), In–Ga–Zn–O (IGZO)[15] and $CuIn_xGa_{1-x}Se$ (CIGS),[16] are used as transparent conductive layers and solar cells, owing to their excellent optical and electronic properties. Their band edge is composed of In5s and In5p orbitals overlapped with p orbitals of anions, which contribute to the optical absorption and electronic conductivity. The excellent optical and electronic properties of indium compounds are also attractive for photocatalysis. Indeed, In_2S_3 is reportedly used as a photocatalyst in organic compound decomposition.[17] $NaInS_2$ with layered rocksalt structure is reported as a photocatalyst for H_2 evolution.[18] Ogisu et al. have reported the photocatalytic activity of a lanthanum-indium oxysulfide, $LaInS_2O$, for H_2 and O_2 evolution.[19] X-ray diffraction peaks of $LaInS_2O$ have been assigned as the orthorhombic cell with a=20.5421(6) Å, b=14.8490(4) Å, c=3.9829(1) Å[20]. However its crystal structure has not been solved. In contrast, more complicated lanthanum indium oxysulfides, $La_5In_3S_9O_3$[20] and $La_6In_{10}S_9O_{17}$[21], have been synthesized and their crystal structures solved by single-crystal XRD.

In this paper, we report a novel layered indium oxysulfide, $LaOInS_2$, whose crystal structure is different from the reported orthorhombic $LaInS_2O$.[20] This layered $LaOInS_2$ is synthesized by a metathesis reaction between LaOCl and $NaInS_2$ with the formation of NaCl as a byproduct. $LaOInS_2$ consists of alternately stacked In–S and La–O layers. The characteristic of the In–S plane is the splitting of In sites with abnormally large anisotropic atomic displacement factors. This is a semiconductor with the band gap of ~2.5 eV where In5s/5p–S3p orbitals dominantly contribute to the bands near the band gap. A photocatalytic activity test shows H_2 and O_2 evolution under visible light.

[a] *Graduate School of Engineering Hokkaido University Kita-13, Nishi-8, Kita-ku, Sapporo 060-8628 Japan.* **E-mail**: amiura@eng.hokudai.ac.jp
[b] *Department of Chemistry, School of Science, Tokyo Institute of Technology, 2-12-1-NE-2 Ookayama, Meguro-ku, Tokyo 152-8550, Japan.* ***E-mail***: maedak@chem.titech.ac.jp
[c] *Research Fellow of Japan Society for the Promotion of Science, 5-3-1 Kojimachi, Chiyoda-ku, Tokyo 102-0083, Japan.*
[d] *Department of Electrical and Electronic Engineering, Tokyo Metropolitan University, 1-1 Minami-osawa, Hachioji, Tokyo 192-0397 Japan.*
[e] *Department of Physical Science, Hiroshima University, 1-3-1 Kagamiyama, Higashihiroshima, Hiroshima 739-8526 Japan.*
[f] *State Key Laboratory of Coal Conversion, Institute of Coal Chemistry, Chinese Academy of Sciences, Taiyuan 030001, P. R. China.*
[g] *National Energy Center for Coal to Clean Fuels, Synfuels China Co., Ltd., Huairou District, Beijing 101400, P. R. China.*
[h] *Center for Crystal Science and Technology, University of Yamanashi, 7-32 Miyamae, Kofu 400-8511 Japan.*

† Footnotes relating to the title and/or authors should appear here.
Electronic Supplementary Information (ESI) available: [details of any supplementary information available should be included here]. See DOI: 10.1039/x0xx00000x

Results and discussion

Synthesis and Crystal Structure

Layered $LaOInS_2$ was synthesized in the evacuated quartz tube by the reaction of LaOCl with $NaInS_2$. At 700 °C, no reaction occurs; only the peaks of LaOCl and $NaInS_2$ phases are observed in the XRD pattern (Fig. 1). The increase to 800 °C starts to form layered $LaOInS_2$ phase. The temperature of 850 °C produces the layered $LaOInS_2$ as the main phase, and NaCl as the by-product. The powder after washing with distilled water shows similar $LaOInS_2$ peaks but does not show the peaks of NaCl.

The reaction for the formation of $LaOInS_2$ is below;

$$LaOCl + NaInS_2 \rightarrow LaOInS_2 + NaCl \quad \text{eq. (1)}$$

Through density functional theory (DFT) calculations using the PBE method, the calculated enthalpy change of the solid-state reaction of eq. (1) at 0 K was slightly endothermic (ca.0.07 eV); the reaction might be thermodynamically unfavorable. However, above melting point of NaCl (801 °C), the reaction of eq. (1) would be thermodynamically favorable due to NaCl liquid with relatively high entropy. The heating at 850 °C of the mixture of La_2O_3, La_2S_3, and In_2S_3 in stoichiometric molar ratio, which did not involve the formation of NaCl, gave no diffraction peaks of $LaOInS_2$. Thus, the formation of $LaOInS_2$ phase above 800 °C from LaOCl and $NaInS_2$ can be explained by the formation of NaCl liquid as a byproduct. The heating at 900 °C caused the decomposition of the layered $LaOInS_2$ into unknown phase(s). Thus, this layered $LaOInS_2$ is a metastable phase which is stable below 900 °C. The diffraction peaks of the product from La_2O_3, La_2S_3, and In_2S_3 and unknown phase(s) decomposed from $LaOInS_2$ were similar to the diffraction patterns of previously reported orthorhombic cell; the structure has not been solved.[20]

Fig. 2 shows a scanning electron microscopy (SEM) image of $LaOInS_2$. Plate crystals 1–10 μm in size and ~1 μm in thickness were found. The BET surface area of the crystals was 0.3 $m^2 \cdot g^{-1}$. The chemical composition of $LaOInS_2$, obtained after washing by water to remove NaCl, is close to the stoichiometric value of $LaOInS_2$; the molar ratio of La:In:S:Na:Cl was 1:0.9:1.8:0.1:0.1, as semiquantitatively determined by energy-dispersed X-ray spectroscopy (EDX). Small amount of Na and Cl were detected; however, the Na amount can be overestimated due to overlapping La and O signals. Thus, we cannot deny the possibility that a small amount of Na and/or Cl is included in the layered structure, or that NaCl byproducts are not completely removed by the water wash.

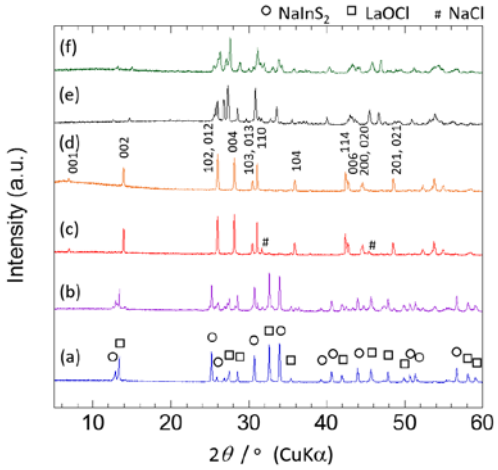

Fig. 1 XRD patterns of the products from the mixture of LaOCl and $NaInS_2$ heated at (a) 700 °C, (b) 800 °C and (c) 850 °C. (d) XRD pattern of the above mixture heated at 850 °C and subsequent wash by water. (e) XRD pattern of pattern of the mixture of La_2S_3, La_2O_3 and In_2S_3 heated at 850 °C and (f) the pattern of above mixture of LaOCl and $NaInS_2$ heated at 900 °C.

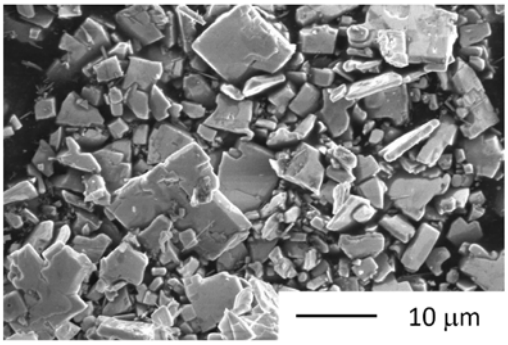

Fig. 2 SEM image of $LaOInS_2$ powder after washing with water.

Journal Name

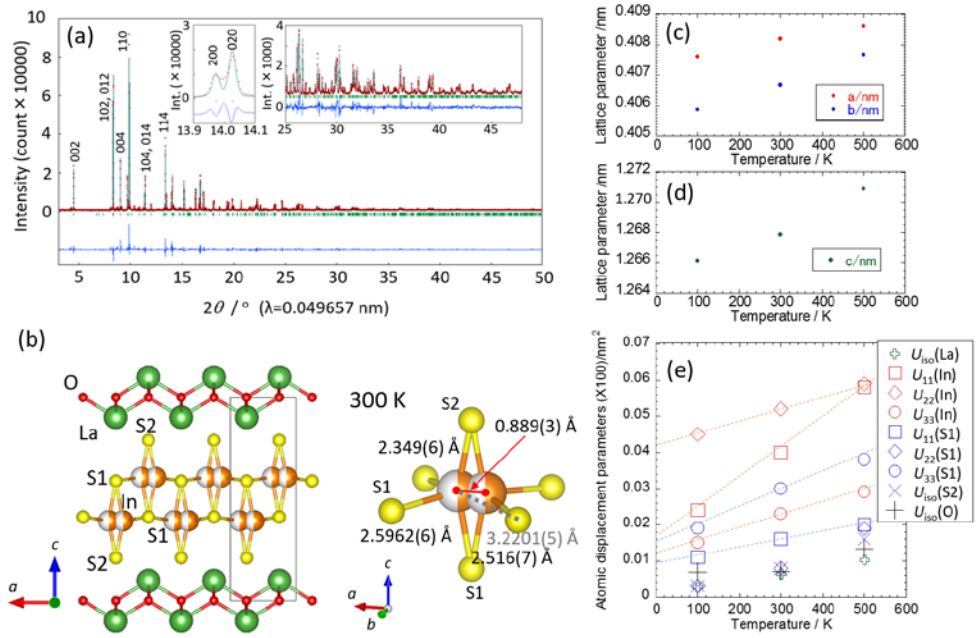

Fig. 3 Crystal structure and Rietveld refinement profile of $LaOInS_2$. (a) Rietveld profile of synchrotron X-ray diffraction of $LaOInS_2$ at 300 K. Red dots and black lines indicate experimental and calculated points. Residuals are indicated by blue lines. Insets are expanded profiles of 200 and 020 peaks and high angle regions. (b) Crystal structure model of $LaOInS_2$ and In-S_6 octahedron. Grey lines indicate the unit cell(c-e) Temperature dependence of lattice parameters and atomic displacement parameters. Anisotropic atomic displacement parameters are refined only for In and S1 (U_{12}, U_{13}, and U_{23} are fixed as zero).

Fig. 3(a) shows the Rietveld profile of layered $LaOInS_2$ after washing with water. Preliminary refinement using a tetragonal cell isostructural with $LaOBiS_2$ produced poor fitting: a reliability factor, R_{wp}, was 32.7 %. An obvious peak split for the 200 and 020 peaks were found (inset of Fig.3(a)), suggesting lowering symmetry from the tetragonal cell. The refinements using orthorhombic cells were attempted, but not successful. Thus, we used the monoclinic cell with the space group of $P2_1/m$(#11). The refinement of β was 90° within the error, thus it was fixed for further refinements. The refinement with this monoclinic cell using slightly different a and b axes significantly improved the fitting (R_{wp} = 17.0 %). However, this refinement converged with an extremely large atomic displacement parameter of In (U_{iso}= 0.098(2) nm^2). The splitting of the central In site into two sites along the a axis improved the fitting (R_{wp} = 13.3 %), and gave a much smaller displacement factor (U_{iso} = 0.038(2) nm^2). Trial refinements with the structural model containing both center and off-centered sites were not converged with reasonable atomic displacement factors. Through DFT calculations using the PBE method, the energy of the optimized structures of $LaOInS_2$ with off-centered In site was determined to be more stable by 0.09 eV than one with centered In site. Such splitting in In sites are also found in $La_5In_3S_9O_3$ and $La_6In_{10}S_9O_{17}$.[20, 21] Therefore, we propose a layered $LaOInS_2$ structure with split In sites in InS_6 octahedron. Final refinement was performed using anisotropic atomic displacement factors of layered In and S1 (R_{wp} = 13.2 %).

Lattice parameters and atomic displacement parameters of $LaOInS_2$ at 100, 300, and 500 K are summarized in Fig. 3 (c-e and Fig. S1). The lattice parameters and the atomic displacement parameters increase with increasing temperature. On the other hand, the asymmetry of a and b axes and anisotropic displacement parameters of U_{11} and U_{22} decrease with increasing temperature. The thermal factors of In and S1 are abnormally high. The extrapolation of the temperature dependence of displacement parameters for In and S1 does not reach zero at 0 K. This indicates the unusual atomic vibrations of the In-S1 layers in the InS_6 octahedron, similar to the structurally related $LaOBi(S,Se)_2$.[13]

Many oxychalcogenides consisting of alternative PbO-type Ln–O layers (Ln: lanthanoid metals) and MCh_2 layers (Ch: S, Se) with trivalent cations (M: Ga^{3+}, In^{3+}, Sb^{3+}, Bi^{3+}) have been reported. Interestingly, there are four-, five-, and six-coordinated MS_2 layers that have been formed within the Ln-O layers (Fig. S2). Simple one is $CeOBiS_2$, which is crystallized in a tetragonal structure.[22] Bi–S layer consists of Bi^{3+}-centered square pyramids, and two Bi–S layers are separated by ~3.35 Å due to the lone-pair of Bi^{3+}. High displacement factors of in-plane S1 are found, especially parallel to the c-axis. The atomic distances of BiS_5 pentahedron are 2.525(3) and 2.8459(3) Å. The electronic bands near the band edge consist of Bi6p and S3p orbitals, and Bi6s is localized. In the case of $LaOInS_2$, two In–S layers are strongly bonded (2.48 Å) and form octahedral sites, where in-plane symmetry of the a and b axes breaks. The In site splits into two sites and forms a pseudo-tetragonal structure. Large atomic

displacement parameters of In toward in-plane direction and those of out-of-plane direction of S1 are found. The atomic distances of InS_6 octahedron range from 2.349(6) Å to 2.5962(6) Å. $LaOGaSe_2$ is crystallized in an orthorhombic structure and is composed of $GaSe_2$ corner-sharing tetragonal chalcogenide layers.[23] Although the *a* and *b* axes are not symmetric, no site-splitting sites of Ga are found. The interlayer distance is close (2.29 Å). The atomic distances of $GaSe_4$ are in the narrow range from 2.440(6) Å to 2.320(6) Å. Therefore, upon changing from $CeOBiS_2$ through $LaOInS_2$ to $LaOGaSe_2$, the interlayer distances, deviation of bond length, and average distance are decreased.

These structural changes of chalcogenide layers would be related to lone pairs, ionic radii, and electronegativity. Cations with lone pairs of s orbitals, such as Bi^{3+}, forms two well-separated layers since they need the space for occupying their lone pairs. Structural analyses of $LnOBiCh_2$,[22, 24] $Ln(O,F)BiCh_2$,[9-13] and $Ln(O,F)SbS_2$[25] show the same trends. On the other hand, for cations without a lone pair, such as Ga^{3+} and In^{3+}, the two chalcogenide layers are strongly bonded. The coordination change from InS_6 octahedron to $GaSe_4$ tetrahedron can be understood by the ratio of ionic radii[26] and the difference of electronegativity.[27] Employing six-coordinated Shannon ionic radii, the ratio of In^{3+}/S^{2-} (0.435) is higher than the critical radius ratio of a six-coordinated species (0.4142) in three-dimensional structures while that of Ga^{3+}/Se^{2-} (0.319) is lower than the critical radius ratio. Employing the difference in electronegativity[28] and the structural map proposed by E. Mooser and W.B. Pearson,[27] the difference in the electron negativity, $\Delta\chi$, of both In–S and Ga–Se are located near the boundary of four- and six-coordinated structures. Nonetheless, slightly larger difference can be found in In-S ($\Delta\chi$ =0.80) than Ga–Se ($\Delta\chi$ =0.74); thus, more ionic character and greater preference for six coordination are expected for the In-S layer. Therefore, structural changes of chalcogenide layers in two-dimensional $LnOMCh_2$ follow the common structural rules based on three-dimensional structures.

Light-absorption property and electronic band structures

Photograph and optical absorption spectrum of the $LaOInS_2$ powder are shown in Fig. 4. $LaOInS_2$ powder is yellow, indicating optical absorption of visible light. The band gap of $LaOInS_2$, using a Tauc plot and assuming a direct transition, is 2.64 eV.

Fig. 5 shows the band structure and projected density of states pDOS of $LaOInS_2$ with off-centered In sites calculated by the HSE06 method. The band structure of $LaOInS_2$ is composed of dispersed conduction and valence bands in the in-plane direction, which is characteristic of layered compounds. At the G and Z points, the band gap is close to minimum, and it is a direct band gap of ~2.4 eV, which is close to the band gap estimated by optical absorption (2.64 eV). This valence-band top is mainly attributed to the S 3p and O 2p orbitals. The bottom of the conduction band consists of In 5s and In5p orbitals. Presence of more dispersed states for In and S than for La and O suggests more covalent character of the In–S layer, as expected. The calculated absorption coefficient under visible light is below 10^4 cm^{-1}, which is not high as InP and CdS.[29]

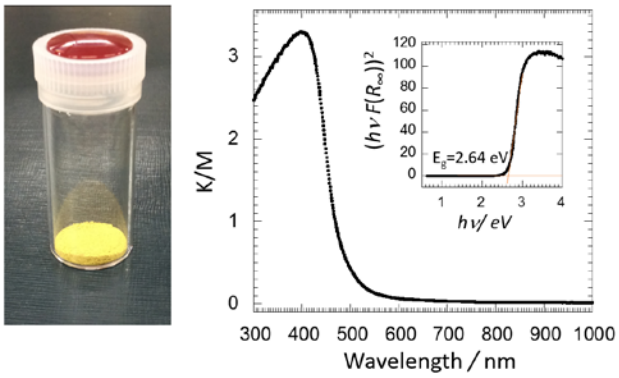

Fig. 4 Photograph and optical absorption of $LaOInS_2$ powder. Inset shows the Tauc plot.

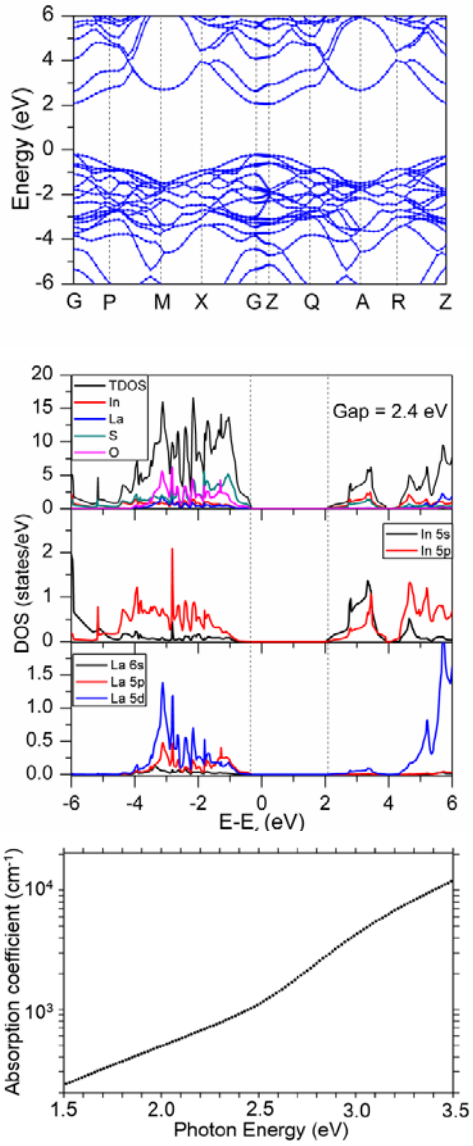

Fig. 5 Computationally calculated band structure, pDOS and absorption coefficient of $LaOInS_2$.

Photocatalytic activity

The well-dispersed valence and conduction bands, as well as visible light absorption of $LaOInS_2$, are attractive for use as a photocatalyst. Photocatalytic activity of $LaOInS_2$ was thus evaluated with respect to H_2 and O_2 evolution from water. Pt nanoparticle was deposited as a cocatalyst for proton reduction. Fig. 6 shows that $LaOInS_2$ was capable of producing H_2 from water containing sacrificial electron donors (Na_2SO_3 and Na_2S) under visible light irradiation of $420 < \lambda < 800$ nm. The H_2 evolution activity was improved with an increase in the loading amount of Pt, reaching a maximum at 0.75 wt%, beyond which it began to drop (Fig. S3). TEM observation for the optimized sample indicated that the deposited Pt was in the form of nanoparticles having ca. 2 nm in size (Fig. S4). Apparent quantum yield of the optimized sample for H_2 evolution was determined to be 0.2% at 420 nm (Fig. S5). It was also confirmed that the H_2 evolution was driven by light absorption of $LaOInS_2$. Even under $500 < \lambda < 800$ nm irradiation, H_2 evolution was clearly observed while no H_2 was evolved under $580 < \lambda < 800$ nm irradiation (Fig. S6). This change in the H_2 evolution activity is consistent with the optical absorption of $LaOInS_2$. No significant degradation of $LaOInS_2$ phase after the H_2 evolution was confirmed by XRD data (Fig. S7). XPS showed no significant change in the peak positions of La3d, In3d, S2p and O1s signals, indicating the surface of $LaOInS_2$ (at least partially) sustained after the photocatalytic test (Fig S8). However, the shoulders of In3d signals at lower binding energy appeared, suggesting the partial reduction of indium. The signal of S2p became broader, which implied the generation of different S species on the surface, although the detailed structure was still unclear.

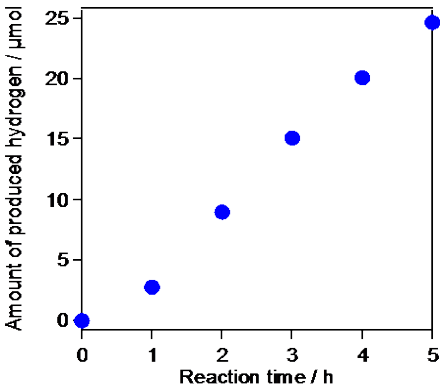

Fig. 6 Time course of H_2 evolution on 0.75 wt% Pt/$LaOInS_2$ under visible light irradiation ($420 < \lambda < 800$ nm). Reaction conditions: catalyst, 50 mg; aqueous methanol solution (10 vol%, 140 mL); light source, xenon lamp (300 W) with cutoff filter; reaction vessel, Pyrex top-irradiation type.

It is known that water oxidation into O_2 by sulphide-based photocatalysts is generally difficult because the valence band of sulphides is formed by S3p orbitals that are more susceptible to oxidation than water.[30] On the other hand, the valence band of oxysulfides consists of hybridized orbitals of S3p and O2p, which may lead to stable photocatalytic behaviour in water oxidation.[6] Thus, we examined photocatalytic O_2 evolution activity of $LaOInS_2$ in the presence of $AgNO_3$ an electron acceptor and La_2O_3 as a pH buffer.[5,6] While no O_2 was evolved using unmodified $LaOInS_2$, modification of $LaOInS_2$ with colloidal IrO_2 as a water oxidation cocatalyst resulted in clearly observable O_2 evolution under visible light ($420 < \lambda < 800$ nm), as shown in Fig. 7. This result indicates that $LaOInS_2$ satisfies the thermodynamic potential to oxidize water into O_2 as well as to reduce water to H_2. The rate of O_2 evolution decreased with time due to the deposition of metallic Ag, which hinders light absorption by $LaOInS_2$ and blocks active sites for redox reactions, as the result of reduction of Ag^+.[6] The deposition of metallic Ag was confirmed by XRD analysis (Fig. S9). It is also clear that the peaks of $LaOInS_2$ phase after the O_2 evolution were sustained after O_2 evolution. However, detailed XPS analysis of the reacted photocatalyst was difficult, because of mixing of $La(OH)_3$, which resulted from the La_2O_3 buffer. We could not remove the $La(OH)_3$ residue by a conventional acid treatment,[5,42] due to chemical instability of $LaOInS_2$ in an acidic solution.

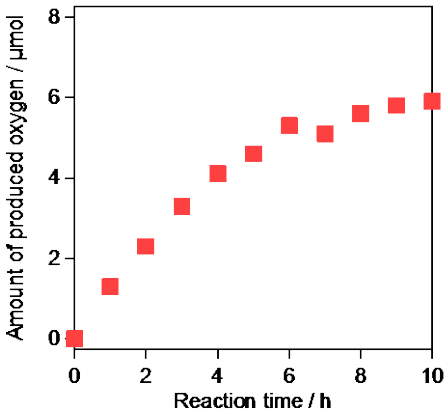

Fig. 7. Time courses of O_2 evolution on 0.5 wt% IrO_2/$LaOInS_2$ under visible light ($420 < \lambda < 800$ nm) from silver nitrate solution containing 200 mg of La_2O_3. Reaction conditions: catalyst, 50 mg; reactant solution, aqueous silver nitrate solution (10 mM, 100 mL); light source, xenon lamp (300 W) with cutoff filter; reaction vessel, top-irradiation type.

The H_2 evolution activity of $LaOInS_2$ was much lower than that of sulphides, such as CdS, with quantum yields of several tens percent.[31, 32] Although there are some early reports that describe photocatalytic water oxidation by sulfides, recent studies showed that sulfides were essentially inactive for photooxidation of water.[6] Therefore, this layered oxysulfide, $LaOInS_2$, is advantageous over other sulfides in terms of the abilities to reduce and oxidize water.

Conclusions

A novel layered oxychalcogenide, $LaOInS_2$, was synthesized by the reaction of LaOCl and $NaInS_2$, with the formation of NaCl liquid as a byproduct. Its crystal structure, electronic structure, optical and photocatalytic properties were examined. It exists as a metastable phase, and its crystal structure can be described as alternately stacked Ln–O oxide and In–S chalcogenide layers. This stacking is similar to those in $CeOBiS_2$ and $LaOGaSe_2$, while octahedral coordination of InS_2 layer is different from the five-coordinated BiS_2 layer in $CeOBiS_2$ and the four-coordinated $GaSe_2$ layer in $LaOGaSe_2$. $LaOInS_2$ is a semiconductor and its band gap, estimated by optical absorption, is 2.64 eV, which is

close to the computationally predicted value (2.5 eV). The bottom of the conduction band is predominantly composed of In 5s/p orbitals, and the valence band mainly consists of O 2p and S3p orbitals. Hydrogen and oxygen evolution from water was confirmed under band-gap photoexcitation of $LaOInS_2$. Tunable electronic structure of $LaOInS_2$ by replacing La, O and S sites suggests that $LaOInS_2$ can be a start point for exploring new functional materials, similar to extensively studied $LaOBiS_2$ and related oxychalcogenides[33]

Experimental and Computational

Synthesis and structural and compositional analysis

The following chemicals were used without purification: $LaCl_3{\cdot}6H_2O$ (Wako>97.0%), $In(NO_3)_3{\cdot}nH_2O$ (Wako 99.9 %) and $NaSH{\cdot}nH_2O$ (Sigma-Aldrich). First, LaOCl was synthesized by heating ~1 g of $LaCl_3{\cdot}6H_2O$ at 820 °C in a N_2 flow, similar to the literature.[34] $NaInS_2$ was synthesized by heating ~1 g of $In(NO_3)_3{\cdot}nH_2O$ and ~2 g of $NaSH{\cdot}nH_2O$ in a Teflon-lined autoclave at 200 °C. After heating, the precipitate was washed with distilled water to remove excess NaSH and byproducts, and dried at 50 °C. The synthesized LaOCl and $NaInS_2$ were mixed in Ar atmosphere. This mixture was heated in a vacuumed quartz tube at 700-900 °C for 4 h. To remove NaCl byproduct, the product was washed with distilled water and dried at room temperature. For comparison, the mixture of La_2S_3, La_2O_3, and In_2S_3 in the molar ratio of 1:2:3 was heated at 850 °C in a vacuumed quartz tube.

The crystal structure was examined by powder X-ray diffraction (XRD: Rigaku Miniflex600). Synchrotron XRD was measured using the one-dimensional semiconductor detector (MYTHEN) at the BL02B2 experimental station in SPring-8 (Proposal number of 2016B1078). Rietveld refinements were performed using RIETAN-FP[35], and a crystal scheme was drawn using VESTA[36]. Diffuse reflectance spectrum was obtained using a UV-vis-NIR spectrophotometer (JASCO V-670). Morphology was observed by SEM (JEOL JSM-6510LA) and transmission electron microscopy (TEM: JEOL, JEM-2010), and chemical compositions were semiquantitatively determined by EDX. Surface area was measured by N_2 absorption experiments. Surface of the powders was examined by XPS (JEOL, JPS-9200). The binding energies were corrected by reference to free carbon (284.6 eV).

Computational calculation

Band structure, density of electron states, and optical absorption coefficient were calculated by density functional theory (DFT) employing the VASP package[37, 38] with HSE06 method[39, 40]. The electron-ion interaction was described by the projector augmented wave (PAW) method with energy cutoff of 400 eV[41]. The convergence criteria for all calculations were set for the electronic self-consistent iterations and forces with 10^{-5} eV and 0.02 eV/ Å respectively. The Gama-point-centered Monkhorst–Pack (MP) (5×5×2) k-mesh scheme[42] was used for structure optimization and density of states (DOS) and dielectric function calculations. The high asymmetry k-points were chosen for band structure calculations. About the optical properties, the imaginary part ($\varepsilon_{Im}(\omega)$) of the frequency dependent dielectric matrix (ε) is determined by a summation over empty states using the converged ground state as following formula,

$$\varepsilon_{\mathrm{Im}}(\omega)=\frac{4\pi^2e^2}{\Omega}\lim_{q\to o}\frac{1}{q^2}\sum_{c,v,k}2\omega_k\delta(\varepsilon_{ck}-\varepsilon_{vk}-\omega)\times\langle u_{ck}+e_\alpha q|u_{vk}\rangle\langle u_{ck}+e_\beta q|u_{vk}\rangle *$$

where the indices c and v refer to conduction and valence band states respectively, ω is the photon energy, and u_{ck} is the cell periodic part of the orbitals at the k-point, k. The real part ($\varepsilon_{\mathrm{Re}}(\omega)$) of the dielectric tensor is obtained by the Kramers-Kronig transformation.

$$\varepsilon_{\mathrm{Re}}(\omega)=1+\frac{2}{\pi}P\int_0^\infty\frac{\varepsilon_{\mathrm{Im}}(\omega')\omega'}{\omega'^2-\omega^2+i\eta}d\omega'$$

Then, the adsorption coefficient ($\alpha(\omega)$) was obtained from the dielectric function by the expression:

$$\alpha(\omega)=\sqrt{2}\omega\sqrt{\sqrt{\varepsilon_{\mathrm{Re}}{}^2(\omega)+\varepsilon_{\mathrm{Im}}{}^2(\omega)}-\varepsilon_{\mathrm{Re}}(\omega)}$$

More details can be found in the work of Gajdoš et al.[43]

Deposition of IrO_2 cocatalysts for photocatalytic water oxidation

Colloidal IrO_2 having 1–2 nm in size was prepared according to the same method reported previously.[44] Because direct adsorption of the prepared IrO_2 colloids onto $LaOInS_2$ was unsuccessful, $LaOInS_2$ (200 mg) was in prior modified with $Ca(OH)_2$ (28 mg, ≥96.0%, Wako Pure Chemical Co.) by an impregnation method in methanol (2 mL, ≥ 99.8%, Kanto Chemical Co.).[6] After drying the suspension, the resulting solid ($Ca(OH)_2/LaOInS_2$) was subject to heating at 573 K for 1 h under a flow of N_2 (100 mL min^{-1}). Then, the heated sample was dispersed in colloidal IrO_2 (0.5 wt%) aqueous solution overnight. This procedure allowed for quantitative adsorption of IrO_2 onto $Ca(OH)_2/LaOInS_2$. For simplicity, the as-prepared material will be represented hereafter as $IrO_2/LaOInS_2$.

Photocatalytic H_2 and O_2 evolution reactions

Photocatalytic activity was evaluated at room temperature in a top-irradiation-type reaction cell connected to a closed gas circulation and evaluation system. The details of the reaction setup can be found elsewhere.[45] For H_2 evolution, $LaOInS_2$ powder synthesized at 850 °C (50 mg) was suspended in 140 mL of an aqueous solution containing 10 mM Na_2S (≥98.0%, Wako Pure Chemical Co.) and 10 mM Na_2SO_3 (≥95.0%, Wako Pure Chemical Co.) as electron donors. Pt (0.1~1.0 wt%) was loaded on $LaOInS_2$ by an in-situ photodeposition method using $H_2PtCl_6{\cdot}6H_2O$ (Kanto Chemical Co., 98.5+%) as the precursor. For water oxidation to O_2, 50 mg of $IrO_2/LaOInS_2$ was dispersed in 100 mL of an aqueous $AgNO_3$ (≥99.8%, Wako Pure Chemical Co.) solution (10 mM) containing 200 mg of La_2O_3, which buffers reaction pH (8–8.5) during the reaction.[6] La_2O_3 (≥99.9 %, Tokyo Chemical Industry Co., Ltd.) was calcined at 1273 K for 2 h in air to remove carbonate and/or hydroxide phases prior to use. The suspension was thoroughly degassed and then exposed to argon (5 kPa). The suspension was irradiated using a Xe lamp (300 W, output current 20 A) fitted with a cold mirror (CM-1) and a cutoff filter to eliminate UV light. The evolved gases were

analyzed by online gas chromatography. When wavelength dependence was examined, a different cutoff filter was used with 10 A output current of the Xe lamp.

The apparent quantum yield (AQY) for H_2 evolution was estimated as

$$AQY(\%) = (A \times R/I) \times 100$$

where A, R, and I represent coefficients based on the reactions (H_2 evolution, 2), the H_2 evolution rate, and the rate of incident photons, respectively. The total number of incident photons (6.8 mW) was measured using a powder meter.

Acknowledgements

We thank Prof. T. Nakanishi and Prof. Y. Hasegawa for optical absorption measurements, and Prof. Yongming Wang for TEM observation. SEM and XPS analyses were conducted at Laboratory of XPS analysis, Hokkaido University. The experiments were partially supported by KAKENHI Grant Numbers 15K14113, 16H04493, 16J10084 and 16K06441.

References

1. S. D. N. Luu and P. Vaqueiro, *Journal of Materiomics*, 2016, **2**, 131-140.
2. S. J. Clarke, P. Adamson, S. J. C. Herkelrath, O. J. Rutt, D. R. Parker, M. J. Pitcher and C. F. Smura, *Inorg. Chem.*, 2008, **47**, 8473-8486.
3. J. R. Panella, J. Chamorro and T. M. McQueen, *Chem. Mater.*, 2016, **28**, 890-895.
4. Y. Goto, J. Seo, K. Kumamoto, T. Hisatomi, Y. Mizuguchi, Y. Kamihara, M. Katayama, T. Minegishi and K. Domen, *Inorg Chem*, 2016, **55**, 3674-3679.
5. K. Ogisu, A. Ishikawa, Y. Shimodaira, T. Takata, H. Kobayashi and K. Domen, *The Journal of Physical Chemistry C*, 2008, **112**, 11978-11984.
6. A. Ishikawa, T. Takata, J. N. Kondo, M. Hara, H. Kobayashi and K. Domen, *J. Am. Chem. Soc.*, 2002, **124**, 13547-13553.
7. M. Palazzi, C. Carcaly and J. Flahaut, *J. Solid State Chem.*, 1980, **35**, 150-155.
8. K. Ueda, S. Inoue, S. Hirose, H. Kawazoe and H. Hosono, *Appl. Phys. Lett.*, 2000, **77**, 2701-2703.
9. H. Kotegawa, Y. Tomita, H. Tou, H. Izawa, Y. Mizuguchi, O. Miura, S. Demura, K. Deguchi and Y. Takano, *J. Phys. Soc. Jpn.*, 2012, **81**, 103702.
10. A. Miura, M. Nagao, T. Takei, S. Watauchi, I. Tanaka and N. Kumada, *J. Solid State Chem.*, 2014, **212**, 213-217.
11. Y. Mizuguchi, A. Miura, J. Kajitani, T. Hiroi, O. Miura, K. Tadanaga, N. Kumada, E. Magome, C. Moriyoshi and Y. Kuroiwa, *Scientific reports*, 2015, **5**, 14968.
12. A. Miura, M. Nagao, T. Takei, S. Watauchi, Y. Mizuguchi, Y. Takano, I. Tanaka and N. Kumada, *Cryst Growth Des*, 2015, **15**, 39-44.
13. Y. Mizuguchi, A. Miura, A. Nishida, O. Miura, K. Tadanaga, N. Kumada, C. H. Lee, E. Magome, C. Moriyoshi and Y. Kuroiwa, *J. Appl. Phys.*, 2016, **119**, 155103.
14. A. Miura, Y. Mizuguchi, T. Sugawara, Y. Wang, T. Takei, N. Kumada, E. Magome, C. Moriyoshi, Y. Kuroiwa, O. Miura and K. Tadanaga, *Inorg Chem*, 2015, **54**, 10462-10467.
15. K. Nomura, H. Ohta, A. Takagi, T. Kamiya, M. Hirano and H. Hosono, *Nature*, 2004, **432**, 488-492.
16. A. Rockett and R. W. Birkmire, *J. Appl. Phys.*, 1991, **70**, R81-R97.
17. Y. He, D. Li, G. Xiao, W. Chen, Y. Chen, M. Sun, H. Huang and X. Fu, *The Journal of Physical Chemistry C*, 2009, **113**, 5254-5262.
18. A. Kudo, A. Nagane, I. Tsuji and H. Kato, *Chem. Lett.*, 2002, **31**, 882-883.
19. K. Ogisu, A. Ishikawa, K. Teramura, K. Toda, M. Hara and K. Domen, *Chem. Lett.*, 2007, **36**, 854-855.
20. H. Kabbour, L. Cario, Y. Moëlo and A. Meerschaut, *J. Solid State Chem.*, 2004, **177**, 1053-1059.
21. L. Gastaldi, D. Carre and M. P. Pardo, *Acta Crystallographica Section B*, 1982, **38**, 2365-2367.
22. R. Sagayama, H. Sagayama, R. Kumai, Y. Murakami, T. Asano, J. Kajitani, R. Higashinaka, T. D. Matsuda and Y. Aoki, *J. Phys. Soc. Jpn.*, 2015, **84**, 123703.
23. S. Benazeth, M. Guittard and P. Laruelle, *Acta Crystallographica Section C*, 1984, **40**, 345-347.
24. A. Miura, Y. Mizuguchi, T. Takei, N. Kumada, E. Magome, C. Moriyoshi, Y. Kuroiwa and K. Tadanaga, *Solid State Commun.*, 2016, **227**, 19-22.
25. M. Nagao, M. Tanaka, R. Matsumoto, H. Tanaka, S. Watauchi, Y. Takano and I. Tanaka, *Crystal Growth & Design*, 2016, **16**, 3037-3042.
26. J. Toofan, *J. Chem. Educ.*, 1994, **71**, 147.
27. E. Mooser and W. B. Pearson, *Acta Crystallographica*, 1959, **12**, 1015-1022.
28. L. Pauling, *J. Am. Chem. Soc.*, 1932, **54**, 3570-3582.
29. E. D. Palik, *Handbook of Optical Constants of Solids*, Academic Press, Burlington, 2002.
30. K. Maeda and K. Domen, *The Journal of Physical Chemistry C*, 2007, **111**, 7851-7861.
31. N. Bao, L. Shen, T. Takata and K. Domen, *Chem. Mater.*, 2008, **20**, 110-117.
32. W. Zhang, Y. Wang, Z. Wang, Z. Zhong and R. Xu, *Chem Commun (Camb)*, 2010, **46**, 7631-7633.
33. Y. Mizuguchi, *The Chemical Record*, 2016, **16**, 633-651.
34. H. Kämmerer and R. Gruehn, *J. Solid State Chem.*, 1996, **122**, 81-86.
35. F. Izumi and K. Momma, *Solid State Phenom.*, 2007, **130**, 15-20.
36. K. Momma and F. Izumi, *J. Appl. Crystallogr.*, 2008, **41**, 653-658.
37. G. Kresse and J. Hafner, *Physical Review B*, 1993, **47**, 558-561.
38. G. Kresse and J. Furthmüller, *Physical Review B*, 1996, **54**, 11169-11186.
39. J. P. Perdew, K. Burke and M. Ernzerhof, *Phys. Rev. Lett.*, 1996, **77**, 3865-3868.
40. J. Heyd and G. E. Scuseria, *The Journal of Chemical Physics*, 2004, **121**, 1187-1192.
41. P. E. Blöchl, *Physical Review B*, 1994, **50**, 17953-17979.
42. H. J. Monkhorst and J. D. Pack, *Physical Review B*, 1976, **13**, 5188-5192.
43. M. Gajdoš, K. Hummer, G. Kresse, J. Furthmüller and F. Bechstedt, *Physical Review B*, 2006, **73**, 045112.
44. K. Maeda and K. Domen, *Angew Chem Int Ed Engl*, 2012, **51**, 9865-9869.
45. K. Maeda, M. Higashi, D. Lu, R. Abe and K. Domen, *J. Am. Chem. Soc.*, 2010, **132**, 5858-5868.